ORIGINAL RESEARCH ARTICLE

Preparation of Ceramic Foam Filters With a Lithium-Containing Surface

CLAUDIA VOIGT, ALINA SCHRAMM, BEATE FANKHÄNEL, EKATERINA SCHMID, PIOTR MALCZYK, JANA HUBÁLKOVÁ, MICHAEL STELTER, ALEXANDROS CHARITOS, and CHRISTOS G. ANEZIRIS

Hydrogen in aluminum causes the formation of detrimental hydrogen porosity in castings. In order to reduce the formation of hydrogen pores, an approach was targeted using lithium as target for hydrogen. This approach utilizes the affinity of lithium for hydrogen, whereby spodumene (a lithium aluminum silicate) and lithium aluminate were used as lithium providers. Within the scope of this study, the preparation of ceramic foam filters with a coating of lithium-containing raw materials (spodumene) was investigated. Those investigations revealed that the spodumene coating has a detrimental influence on the bending strength of the foams when a certain level of spodumene is exceeded. This observation might be explainable by the intrusion of the spodumene into the alumina matrix of the skeleton foam. Two wetting tests at different temperatures were conducted, verifying the significant influence of the temperature on the reaction between the spodumene and AlSi7Mg. Furthermore, test filters coated with raw materials exhibiting different amounts of lithium were conducted. The hydrogen pores were evaluated by light microscopy and computed tomography. The analyzed pore size distribution in the aluminum did not elucidate the proximate influence of the lithium-coating on the ceramic foam filter on the hydrogen porosity in the aluminum.

https://doi.org/10.1007/s11663-022-02533-2

I. INTRODUCTION

THE mechanical properties of aluminum are directly linked with its purity. The latter, concerning aluminum and its alloys is defined by the amount of hydrogen, non-metallic inclusions, and undesirable trace elements. Hydrogen is the only known gas soluble in aluminum and is one of the main reasons for pore formation in aluminum castings.[1]

Hydrogen sources are wet refractory materials and tools, as well as water vapor from the air.[1,2] The water vapor (moisture) reacts with the aluminum to create alumina and hydrogen Eqs. [1] and [2].[2]

$$2Al + 3H_2O \rightarrow Al_2O_3 + 3H_2, \quad [1]$$

$$H_2 \rightarrow 2[H]. \quad [2]$$

The diatomic hydrogen dissolves in aluminum to monoatomic atoms [H] and can enter the aluminum microstructure.[1]

The reason for the formation of hydrogen porosity is the change in hydrogen solubility during the solidification of aluminum. The equilibrium hydrogen content of the aluminum melt decreases decisively during its solidification.[1,2] The difference in solubility is caused by the increase in density which is brought about by the decrease in volume whereby the interstitial sites containing hydrogen are compressed, and so the hydrogen is forced out of the aluminum structure into the liquid head of the solidification front. During solidification, the hydrogen level at the solidification front increases, causing a majority of the hydrogen pores in the center of the casting preferably at the position of the last solidification. The hydrogen porosity can arise as interdendritic porosity and microporosity.[3]

According to Talbot,[4] the higher the hydrogen content, the higher the porosity, and the lower the mechanical properties of the solidified aluminum. Therefore, efforts are made to reduce the hydrogen

CLAUDIA VOIGT, PIOTR MALCZYK, JANA HUBÁLKOVÁ, and CHRISTOS G. ANEZIRIS are with the Institute of Ceramics, Refractories and Composite Materials, Technische Universität Bergakademie Freiberg, Agricolastr. 17, 09599 Freiberg, Germany. Contact e-mail: Claudia.voigt@ikfvw.tu-freiberg.de ALINA SCHRAMM, BEATE FANKHÄNEL, EKATERINA SCHMID, MICHAEL STELTER, and ALEXANDROS CHARITOS are with the Institute for Nonferrous Metallurgy and Purest Materials, Technische Universität Bergakademie Freiberg, Leipziger Straße 34, 09599, Freiberg, Germany.

Manuscript submitted December 10, 2021; accepted April 12, 2022. Article published online May 5, 2022.

content in the aluminum melt, for example, by means of gas purging treatments, covering of the aluminum melt, and drying the used tools and added alloying elements. A relatively new approach is the application of reactive ceramic foam filters coated with lithium-containing phases. According to the commercial software FactSage 8.1®, lithium should react with hydrogen; for example, the reaction given by Eq. [3] shows a ΔG° of approximately—96 kJ at a temperature of 750 °C.

$$2Al + 2[H] + 2Li_2O \rightarrow 2LiH + LiAl + LiAlO_2 \quad [3]$$

Thereby, spodumene ($LiAl[Si_2O_6]$ can be expressed also as 0.5 $Li_2O{\cdot}Al_2O_3{\cdot}(SiO_2)_4$) could aid to reduce the hydrogen content of the aluminum. It should be noted that the above ΔG° corresponds to components being in their standard state, *i.e.*, hydrogen as a gas at 1 atm, while rest products and reactants are considered pure and hence as separate phases. The actual activity of hydrogen during filtration is difficult to assess. On the one hand, the activity of dissolved hydrogen in the melt should be rather low, while on the other, the activity of hydrogen at a potential nucleation site on the filter (where hydrogen would be present as a gas) would be approx. 1 (maximum attainable value) and hence hydrogen would be present at its aforementioned standard state.

Should the stability of potentially formed LiH be discussed in terms of the reaction ($LiH \rightarrow Li + [H]$), it is shown that LiH is not stable above 950 °C, since the respective ΔG° of this reaction becomes negative and hence spontaneous (according to FactSage 8.1®) at thermodynamic standard conditions, defined above, where hydrogen is considered as a gas at 1 atm). The decomposition of LiH may occur even at lower temperatures considering the low activity of dissolved hydrogen within the melt. Such an approach to reduce hydrogen porosity in an aluminum melt (according to Eq. [3]) was tested, for the first time, by Fankhänel *et al.*[5–7] with spodumene-coated ceramic foam filters.

Spodumene is an exploitable mineral used as a raw material for lithium extraction and as a sintering aid for producing ceramics, pottery, and glass fibers.[8] The advantage of the ceramic foam filters is their high surface area and the possibility of applying them at the end of the casting process to remove non-metallic inclusions.[9] Thus, by using lithium-containing filters, a double benefit could be obtained—a reduction of the hydrogen content and removal of non-metallic inclusions.

For the measurement of hydrogen in aluminum, a number of methods are available which can be divided in closed-loop recirculation techniques, density index tester and carrier extraction techniques. Closed-loop recirculation techniques (for example, AlSCAN and Telegas) are an online measuring method using a nitrogen carrier gas circulating through the aluminum melt to allow a hydrogen diffusion from the melt into the nitrogen. A measurement of the thermal conductivity of the nitrogen gas allows the determination of the hydrogen content in the aluminum melt.[10,11] Other systems (for example, ALSPEK) use a calcium zirconate as an electrochemical cell for the determination of the hydrogen content in the nitrogen gas. Density index tester compares two samples of liquid metal, the first one solidified under atmospheric and the second sample under vacuum condition. The vacuum leads to the creation of bubbles from the hydrogen present in the aluminum, which leads to a bloating of the sample and results in a lower density. The density ratio of the two samples gives a hint on both inclusion and hydrogen content.[11]

In the case of carrier extraction techniques, the solid aluminum sample is melted and the released hydrogen is measured with, *e.g.*, a non-dispersive infrared analyzer. The sample weight with < 10 g is very small and therefore not significant for large volumes as the hydrogen level is not mandatory evenly distributed. This leads to problems when analyzing larger aluminum volumes.[11] For this reason, a steel mold designed for an accumulation of pores in the upper part of the casting was used in this study. Thus, such setup may allow the examination of larger volumes of aluminum.

This work is aimed to investigate the preparation of ceramic foam filters based on alumina with a lithium-containing surface. Furthermore, the influence of filters with lithium-containing surfaces on the hydrogen porosity of an AlSi7Mg alloy was evaluated, whereby alumina filters were coated with raw materials of different lithium contents. Additionally, wetting experiments at different temperatures were conducted.

II. MATERIALS AND METHODS

A. *Characterization of the Raw Materials*

Three different lithium-containing raw materials were used in this work for wetting tests and the investigations of the influence on the hydrogen porosity (*i.e.*, filtration tests): (i) spodumene 1 from the ceramic supplier Keramik Kraft (Germany), (ii) spodumene 2 (Albemarle), and (iii) a lithium aluminate (Sigma Aldrich). Additionally, spodumene 1 was used for the basic investigations regarding the preparation of ceramic foam filters with a lithium-containing surface.

In the first step, the lithium-containing raw materials were analyzed with an ICP-OES Spectrometer 725 (Varian Inc.) regarding their Li content after a chemical digestion with HNO_3/HF. Every raw material was analyzed two times. Additionally, the raw materials were measured by the differential scanning calorimetry (DSC) STA 409 PC Luxx (Netzsch, Germany) between 20 and 1400 °C with a heating rate of 10 K/min in platinum crucibles. Furthermore, the raw material spodumene 1 was heated in a hot stage microscope (Raczek, Germany) to examine the softening point until a temperature of 1500 °C with a heating rate of 10 K/min. Before the test, the spodumene powder was pressed with 60 MPa to a cylindrical sample with a diameter of 10 mm and exhibiting a height of 3 mm placed on a sintered alumina substrate.

B. *Coating of Ceramic Foam Filters and Substrates with Lithium-Containing Raw Materials*

Preparation of ceramic foam filters exclusively from spodumene is not possible due to the low melting point of the spodumene. Therefore, the alumina skeleton foams ($50 \times 50 \times 20$ mm^3 with 10 pores per inch) as well as Al_2O_3 substrates for hot stage microscopy (diameter 12 mm and height 3 mm), and Al_2O_3 substrates for hot stage microscopy with capillary purification setup (diameter 55 mm and height 3 mm) were coated with slurries containing different lithium sources listed in Table I. Uncoated Al_2O_3 skeleton foams and uncoated Al_2O_3 substrates were used as reference material. The slurries consisting of the lithium-containing raw material, deionized water, Optapix AC 170 (temporary binder), and Gießfix 162 (dispersant) were homogenized by ball milling for at least 20 hours. In the next step, the coating slurries were applied using a combined dip-spin technique where the Al_2O_3 skeleton was immersed into the slurry completely, followed by a centrifugation step for the removal of excess slurry. In order to investigate the influence of the applied amount of spodumene 1 on the bending strength, the solid content of the slurries was varied between 55 and 80 mass pct. After drying the slurry, the coated ceramic foam filters and substrates were thermally treated at temperatures from 1375 °C to 1600 °C regarding to the utilized lithium-containing raw material. The corresponding temperatures of the thermal treatment are given in Table I. By measuring the masses of the coated and thermally treated foam filters and the corresponding uncoated alumina skeletons, the actual mass of the applied lithium-containing material was calculated.

The bending and compression strength of the ceramic foam filters coated with spodumene 1 (thermal treatment at 1375 and 1400 °C) was tested using the mechanical testing device Tiratest 2420 (TIRA GmbH, Germany) at a loading rate of 20 mm/min and a span of 36 mm between the supports for the ceramic foam filters ($50 \times 50 \times 22$ mm^3). The measurement is aborted when a force loss of 70 pct of the maximum force is reached and the maximum force was used for the calculation of the bending strength. At least 25 samples were tested for each batch of samples treated thermally at the respective selected temperature.

In the next step, the presence of lithium was verified by a plasma-based secondary neutral mass spectrometry (SNMS) to make sure that the sintering step of the applied coating did not lead to a complete evaporation of the lithium.[12] This method is based on ion bombardment of the sample and subsequent ionization of the sputtered neutrals. Experiments were performed using the INA-X equipment (SPECS GmbH, Germany).[13] In this configuration, an electron cyclotron wave resonance (ECWR) plasma serves both as source for primary ions and for post-ionization. After passing an ion optic, the post-ionized neutrals are separated by a quadrupole mass analyzer and counted by a secondary electron multiplier. The SNMS measurements were done in the so-called high-frequency mode (HFM) due to the dielectric properties of the investigated samples.[14]

The measurements were conducted at the substrates prepared for the sessile drop measurements which are flat and possess a diameter of ~ 12 mm. Each sample type was measured three times by using a copper mask (5 mm in diameter) positioned on top of the sample. For the measurements, a krypton plasma with 152 W, 4.5 A and working pressure of 2×10^{-3} mbar was used. The applied voltage was set to 500 V at a frequency of 91 kHz and a duty cycle of 60 pct. The distance between the sample surface and the molybdenum aperture during measurements was 1.5 mm. The sputter time for each mass spectrum was 210 seconds.

C. *Wetting Measurements with Aluminum Melt*

For the investigation of the wetting behavior between the ceramic substrates and metal melts, sessile drop tests are often used. In this work, two different sessile drop procedures were applied. In the first step, conventional sessile drop tests were conducted in a high-temperature tube furnace, equipped with a high vacuum pump and an inert gas system (Carbolite Gero, Germany) located at the Institute for Nonferrous Metallurgy and Purest Materials (TU Bergakademie Freiberg, Germany).

The used aluminum alloys were produced by Trimet Aluminium, Germany, and cut into shape immediately before the testing to avoid the buildup of a massive oxide layer.[15] Metal samples weighing < 100 mg were prepared, placed on the substrates coated with the

Table I. Slurry Compositions of the Coating Slurries (*Based on the Sum of Solids)

Raw Materials	Supplier	Al_2O_3 Skeleton + Spodumene 1	Al_2O_3 Skeleton + Spodumene 2	Al_2O_3 Skeleton + Lithium Aluminate
Spodumene 1/Pct	Keramik Kraft	100		
Spodumene 2/Pct	Albemarle		100	
Lithium Aluminate/Pct	Sigma Aldrich			100
Optapix AC 170*/Pct	Zschimmer & Schwarz, Germany	1	1	1
Gießfix 162*/Pct	Zschimmer & Schwarz, Germany	0.6	0.6	0.6
Solid Content/Pct		55 to 80	74	74
Temperature of Thermal Treatment/°C		1375 and 1400	1400	1600

lithium-containing raw materials (diameter 12 mm), and positioned in the furnace at room temperature. The alloy AlSi7Mg was used in combination with substrates made of pure Al_2O_3 as reference, spodumene 2, and lithium aluminate, and AlSi5Mg was investigated in combination with spodumene 1.

Previous experience showed that the different silicon content of both used alloys has no significant influence on their wetting behavior. Every lithium-containing raw material was tested twice. As a reference, a sintered alumina substrate was used. Before starting the heating procedure at 350 K/h to the temperature of 950 °C, the furnace was evacuated to attain a pressure of $p \leq 1.5 \times 10^{-5}$ mbar. After a dwell time of 180 minutes at the maximum temperature, a pressure lower than $p < 8 \times 10^{-6}$ mbar was achieved.

For evaluating the contact angle θ_{cal}, following equation, valid for small droplets (m < 100 mg), was used[16]:

$$\theta_{cal} = 2 \arctan (2 \text{ hour/day}). \quad [4]$$

The height h and the base diameter d of the aluminum droplet were obtained from digital images recorded with a digital camera (The Imaging Source, Germany).

The used test temperature of 950 °C is the lowest usable temperature for conventional sessile drop tests with aluminum due to the strong affinity of aluminum to oxygen. An oxide layer covering the aluminum droplet prevents a direct contact between the liquid aluminum and the substrate and thus falsifies the measured contact angle. The oxide skin decomposes only at temperatures ≥ 950 °C and sufficient vacuum, making the contact angles attained with the conventional sessile drop technique considerably more reliable under these conditions. As the aluminum melt filtration took place at temperatures between 690 and 730 °C, the temperature of the sessile drop tests at 950 °C is significantly higher. In the case of reactive systems (substrate and aluminum), this can lead to falsification of the occurring reactions and incorrect results of the contact angle measurements.[17,18]

For sessile drop tests at lower temperatures, removal of the oxide skin is necessary. This can be accomplished by the application of an adapted dropping device, as, for example, in capillary purification[19] or improved sessile drop technique.[20] In this work, a simplified capillary purification setup with hopper for melting of aluminum and a drop pressing plunger standing on the aluminum sample was used as described by Malczyk *et al.*[21] This capillary setup made of aluminum inert boron nitride (Henze Boron Nitride Products AG, Germany) ensured the mechanical removal of oxide skin from the initial aluminum sample. This capillary setup was placed on top of the substrate (diameter 55 mm and a height of 3 mm) and then positioned in the hot stage microscope. The hot stage was heated at a rate of 10 K/min to a temperature of 730 °C with a holding time of 10 minutes. During heating and holding, the furnace chamber was flushed with argon to decrease the oxygen level. The AlSi7Mg alloy (Trimet Aluminium, Germany) was used for the tests. The drop weight was between 380 and 530 mg, which is significantly higher than in the conventional sessile drop tests, and the deviation was higher. The drawback of the setup shows no adjustability of the dropping temperature due to the missing of a mechanical trigger. The contact angles were measured with a using a FIJI plugin called drop snake.[22]

Due to the differences in the measuring temperature and drop masses between the two utilized testing setups, their measured contact angles were not compared.

D. *Casting Trials and Evaluation of the Porosity in the Cast Aluminum Samples*

For conducting the casting trials with a focus on the hydrogen porosity of the resulting aluminum alloy castings, a special steel mold with a wedge-like geometry and a metal core in the central area has been used as described by Fankhänel *et al.*[5] The uppermost part of the casting solidifies first (fast) thus disallowing significant amounts of hydrogen to escape upon cooling of the rest of the cast. On the contrary, the upper part of the mold is cooled in such a way that promotes a specific solidification behavior (as a result of the metal core presence) resulting in an accumulation of pores in this upper part of the casting if hydrogen is present in the aluminum melt. Before each casting process, the inner surface of the mold is spray-coated with a BN spray release agent HeBoCoat SL-E 125 (Henze Boron Nitride Products AG, Germany).

The prepared ceramic foam filters (alumina, Al_2O_3 + spodumene 1, Al_2O_3 + spodumene 2, and Al_2O_3 + lithium aluminate) were used for filtering the molten AlSi7Mg alloy. Three casting trials with respective filters were performed for each filter type to ensure repeatability of the results.

Before filtration, the sides of the ceramic foam filters were closed off using the refractory paste Kerathin® (Rath Group, Austria), containing ceramic fibers, and dried at room temperature for at least 3 days. This sealing step should avoid the spilling of liquid metal outside of the mold. In the next step, the ceramic foam filter was topped with a ceramic hopper and placed on the top of the mold. Strips of ceramic fiber paper were placed between the mold's top surface and the ceramic foam filter to ensure the evenness of the filter's placement.

The mold and the ceramic foam filters with ceramic hopper were preheated in an electric resistance furnace (MLW VEB Elektro Bad Frankenhausen, GDR) to a temperature of 250 °C to avoid cold shuts and filter clogging during the casting process.

The aluminum alloy was melted down in a graphite-coated crucible, which was placed in an electric furnace (Carbolite Gero, Germany) set to a temperature of 750 °C. According to the measurements of the melt temperature, the casting temperature was always kept at approximately 745 °C.

After removing the oxide and impurity layer from the melt surface with a stainless steel tool, the aluminum melt was manually poured through the respective ceramic foam filter into the preheated mold. In the last step, the aluminum casting was solidified and cooled down to room temperature and unpacked from the casting mold.

The evaluation of the porosity of the cast samples was performed with the help of light microscopy and computed tomography.

The cast samples (Figure 1(a)) were first cut into two pieces (Figure 1(b)). The right piece of the casting sample (see Figure 1(b)) was entirely analyzed by a micro-focus X-ray computer tomograph CT-ALPHA (ProCon X-Ray, Germany) equipped with a 160 kV X-ray tube and a Dexela detector 1512. The resolution (voxel size) of the reconstructed volume images was 41 μm indicating that the smallest detectable pore size is about 100 μm. The reconstructed CT data were analyzed with the software Modular Algorithms for Volume Images (MAVI, Fraunhofer, Germany). The data processing started with a cropping step to choose the region of interest whereby a volume of 360 $\times$ 680 $\times$ 1040 pixel (correspond to approximately 14 $\times$ 27 $\times$ 42 mm^3) was selected for further analysis, see Figure 1 (red areas).

The following binarization step transformed the grayscale image into a black image (background) and white image (foreground) see Figures 2(a) and (b), which was a particularly critical step due to the strong influence on the detected pore size and the challenging definition of the threshold. Furthermore, the occurrence of ring artifacts, due to the size of the aluminum samples, made the selection of a suitable threshold more complicated. After binarization, a labeling step (see Figure 2(c)) on the background and the feature "object analysis" allows the determination of the number and size of the pores. For the visualization of the pore distribution in the analyzed sample, the background was made transparent by the feature "object filter."

For the investigation of the pores smaller than 100 μm, analysis by light microscope was conducted for one sample per cast, see Figure 1 (d)), whereby the sample was taken from the upper part of the wedge-shaped region above the core of the mold. The surface of

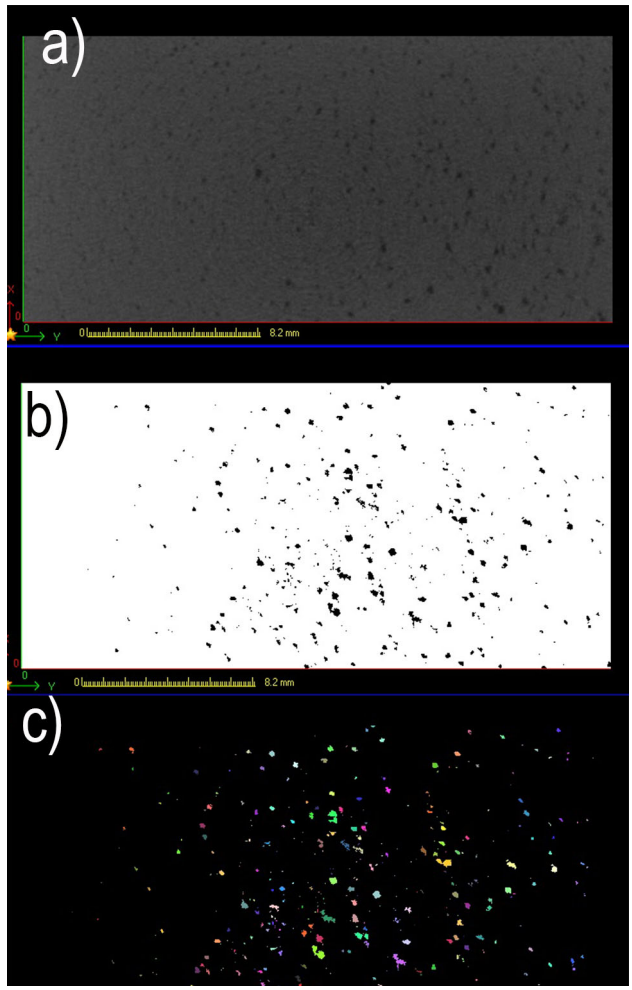

Fig. 2—Data processing from reconstructed computed tomography data (*a*) cropped data, (*b*) binarized, and (*c*) labeled data.

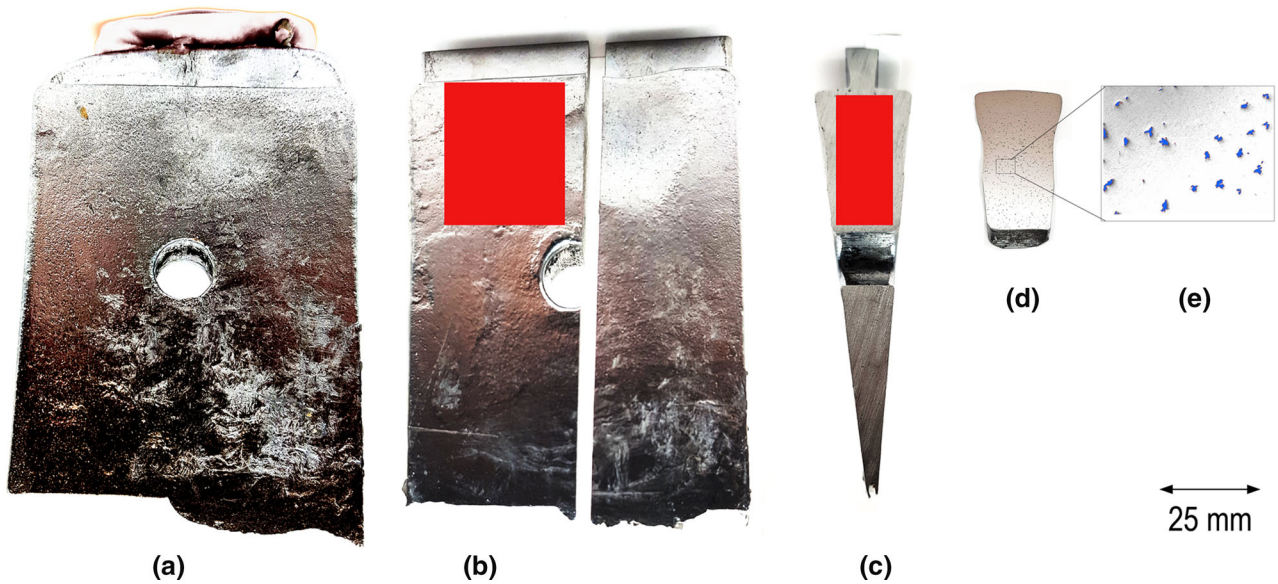

Fig. 1—Aluminum casting sample (*a*) sample after casting, (*b*) sample cut in two pieces—frontal view, (*c*) side view, (*d*) further cut and polished sample for analysis with light microscope, and (*e*) blue areas are the marked pores, the red area was analyzed by computed tomography (Color figure online).

this sample was then polished and evaluated with regard to its pores using a digital optical microscope Axio Imager M2m (Carl Zeiss AG, Germany) along with the evaluation software AxioVision SE64 V4.8 (Carl Zeiss Microscopy GmbH, Germany). Utilizing the contrast between the pores and the surrounding metal, the pores can be quantified and evaluated considering their quantity, size, and shape. Per sample, an area of nearly 200 mm^2 (consisting of 33 measured and merged images with a size of 2829 × 2132 μm^2) was evaluated. The pores were automatically detected, and their number and size were analyzed. With the help of the pore area, an area-equivalent circle diameter was calculated.

III. RESULTS

A. *Characterization of the Raw Materials*

The results of the ICP measurements on the lithium-containing raw materials are listed in Table II and show significant differences in the lithium content. In case of a reaction between the lithium and the hydrogen in the aluminum melt, different hydrogen porosity values would be expected.

The differential scanning calorimetry (DSC) measurements yielded a comparable behavior for the two spodumene samples with a strong decrease at temperatures > 1355 °C (spodumene 1) and > 1316 °C (spodumene 2), see Figure 3. This decrease is the beginning of an endothermic peak which is not completely displayed due to the applicable maximum temperature of 1400 °C of the STA 409 PC Luxx. This endothermic peak indicates the melting temperature of spodumene. Due to the too low applicable temperature, the peak minimum which is the melting temperature is not displayed. According to Salmang *et al.*,[23] the melting temperature of spodumene is 1423 °C.

Table II:. Results of ICP Measurements on the Li Containing Raw Materials

	Li/Mass Percent
Spodumene 1	3.74 ± 0.01
Spodumene 2	1.86 ± 0.01
Lithium Aluminate	9.31 ± 0.03

The lithium aluminate did not show an endothermic peak in the differential scanning calorimetry measurement due to a higher melting temperature than. The melting temperature of lithium aluminate is according to the literature 1610 °C.[24]

In the next step, the softening and melting behavior was investigated with a hot stage microscope. A clear change of the shape of the pressed spodumene 1 was visible at temperatures of 1416 °C and higher, see Figure 4. So, the beginning of melting of spodumene 1

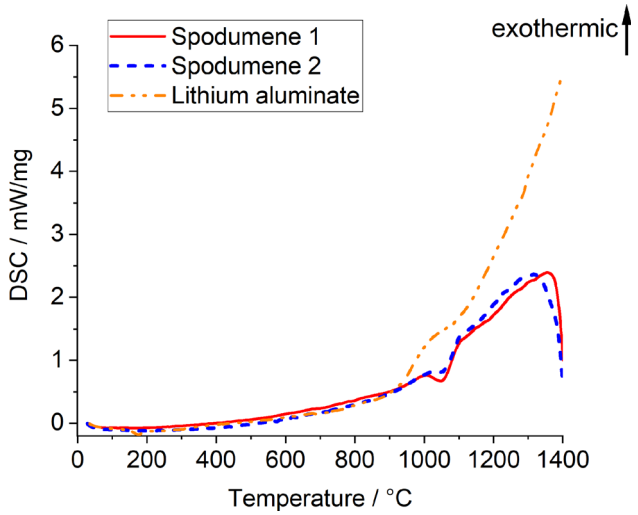

Fig. 3—DSC measurements of the lithium-containing raw materials.

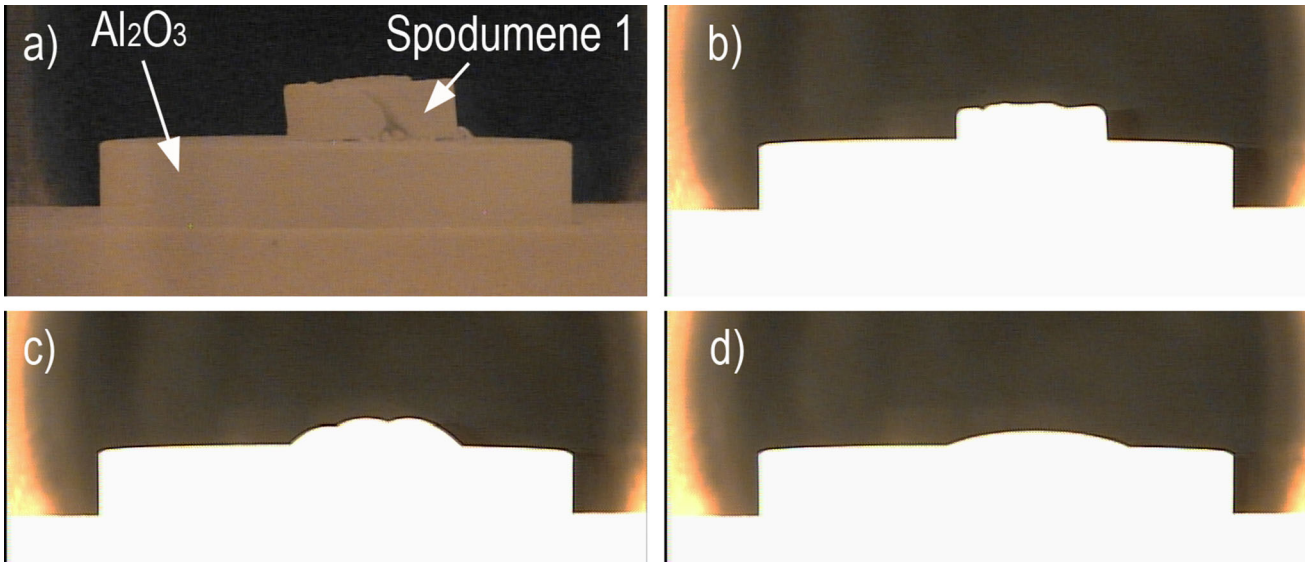

Fig. 4—Hot stage microscopic images (*a*) 1113 °C, (*b*) 1406 °C, (*c*) 1416 °C, and (*d*) 1438 °C.

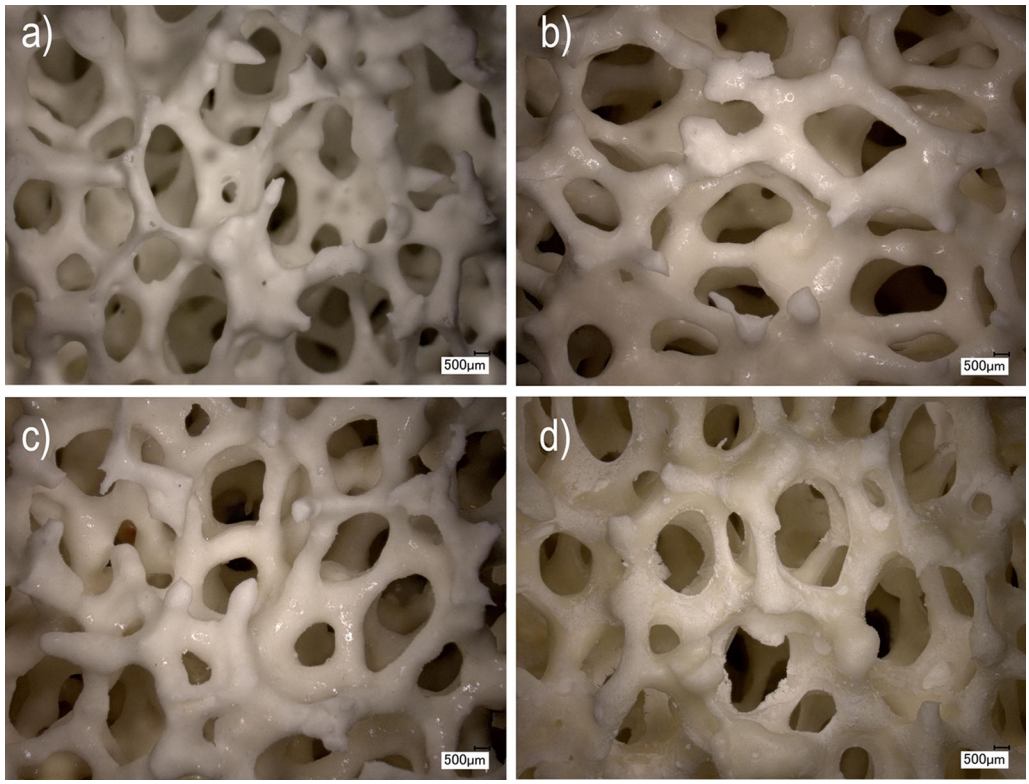

Fig. 5—Light microscopic images of alumina foams (*a*) pure alumina without coating as a reference, (*b*) alumina with spodumene 1 coating thermally treated at 1400 °C, (*c*) alumina with spodumene 2 coating thermally treated at 1400 °C, and (*d*) alumina with lithium aluminate coating sintered at 1600.

was between 1406 and 1416 °C. The apparent decrease of the volume of spodumene 1 was notable, indicating probably an intrusion of the spodumene 1 into the sintered alumina substrate. No formation of bubbles or other irregularities were observed.

B. *Coating of Ceramic Foam Filters and Substrates with Lithium-Containing Raw Materials*

The alumina skeleton foams coated with spodumene 1 and spodumene 2 exhibit a shiny surface caused by the molten and solidified spodumene, see Figure 5. Preliminary investigations with regard to filter thermal treatment performed at 1375 °C showed an incomplete melting of spodumene at 1375 °C resulting in loose particles which could break away during the filtration process. For this reason, the temperature of the heat treatment was set to 1400 °C. The alumina foams coated with lithium aluminate do not possess a shiny surface but an inhomogeneous one—there are white and slightly yellow areas visible. A temperature lower than the melting temperature resulted probably in a sintered but not a melted coating.

Preliminary investigations with alumina foams revealed that spodumene coating resulted in challenges regarding easily breakable foam filters after the thermal treatment of the spodumene. A variety of thermal treatment tests were conducted in which the temperature and atmosphere were varied, resulting in no appreciable improvement. Furthermore, the mass of the applied

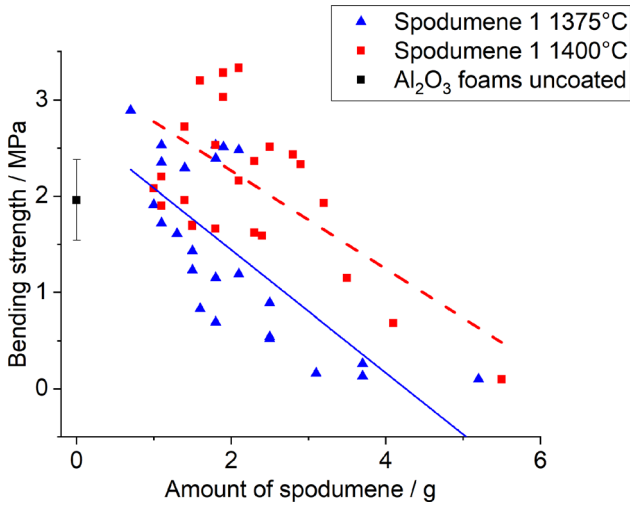

Fig. 6—Bending strength of foams coated with different amounts of spodumene 1.

spodumene was varied by changing the solid content of the coating slurry. This evaluation was conducted with alumina foams coated with spodumene 1. According to Figures 6 and 7, the amount of applied spodumene 1 exhibited a significant influence on the measured bending strength. At the lowest applied amount of spodumene 1 (for 1375 °C until 1.5 g and for 1400 °C until 2.3 g), the bending strength is comparable to uncoated alumina skeleton foams or even higher. A higher

bending strength might be explainable by the closure of existing cracks and imperfections by the spodumene 1 melt. In the case of a higher amount of spodumene 1, the bending strength decreases significantly to values lower than 1 MPa. Furthermore, the compression strength of alumina skeleton foams coated with spodumene was measured and yielded comparable results: The higher the amount of applied spodumene, the lower is the measured compression strength. It should be mentioned that the measured bending and compression strength of uncoated alumina foams are not comparable to industrial produced alumina foams for the aluminum filtration. The alumina foams used in this study are made of pure alumina without any bonding phase whereas industrial foam filters for the aluminum melt filtration are phosphate or silicate bonded with lower strength values.

SEM images clarify the reason for the drop in strength, see Figure 8. Firstly, a coating on the alumina skeleton is not visible. Consequently, the applied spodumene 1 intruded into the alumina skeleton foam, observable as a gray and inhomogeneous phase between the alumina grains. The EDX analysis showed a high silicon content of higher than 40 mass pct at these positions. Lithium is not detectable by EDX due to its low atomic number. The high intrusion of spodumene 1 into the alumina microstructure can be explained by the viscosity decreasing effect attributed to lithium.[25] The strong decrease of the strength is probably caused by a negative coefficient of expansion of the system $Li_2O{\cdot}Al_2O_3{\cdot}SiO_2$ inducing a mismatch with the alumina grains possessing a positive coefficient of expansion.[25] The highly anisotropic coefficient of expansion of $Li_2O{\cdot}Al_2O_3{\cdot}2\ SiO_2$ (*a*-axis $+\ 8{\cdot}10^{-6}\ K^{-1}$ and *c*-axis $-\ 16{\cdot}10^{-6}\ K^{-1}$) is mentioned in literature.[23] In the preparation of the ceramic foam filters for the casting tests, the applied amounts of spodumene 1 were smaller than 1.5 g per tested filter.

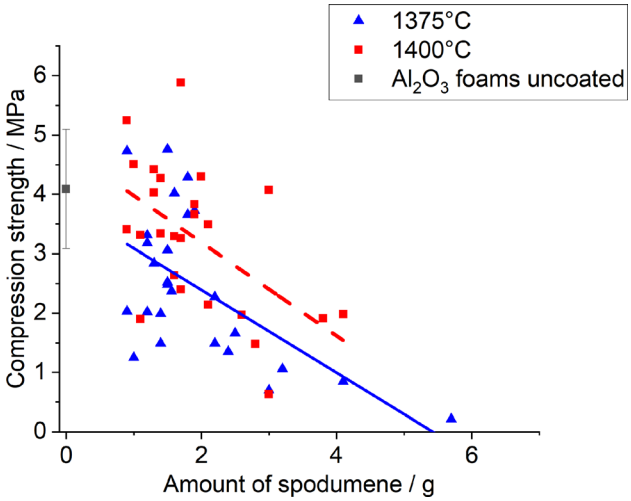

Fig. 7—Compression strength of foams coated with different amounts of spodumene 1.

In the next step, the lithium content of the samples was examined to make sure that the sintering step of the spodumene 1, 2 and the lithium aluminate coating did not lead to a complete evaporation of the lithium. The SNMS measurements were carried out at the surface of coated and sintered substrates used for the sessile drop measurements. Figure 9 shows clear lithium peaks indicating the presence of lithium at the surface of sintered lithium-containing coatings in comparison to pure alumina substrates without any lithium peaks. The deviations in intensity within one sample type are caused among other things by the inhomogeneity of the surface. The measured intensity depends not only on the concentration of the atoms, but also on detection factors which are influenced by geometry factors, post-ionization probability, and transmission factors.[26,27] For this reason, a quantification of the lithium content would be only possible after referencing the lithium-containing components and is therefore not part of this work.

C. *Wetting Measurements with Aluminum Melt*

The conventional sessile drop tests at 950 °C show a decreasing contact angle at increasing contact time caused by the decomposition of the oxide skin,[16,20] see Figure 10. According to literature, the reference alumina sample did not show any reaction with the AlSi7Mg melt[28] and exhibited a typical development of the

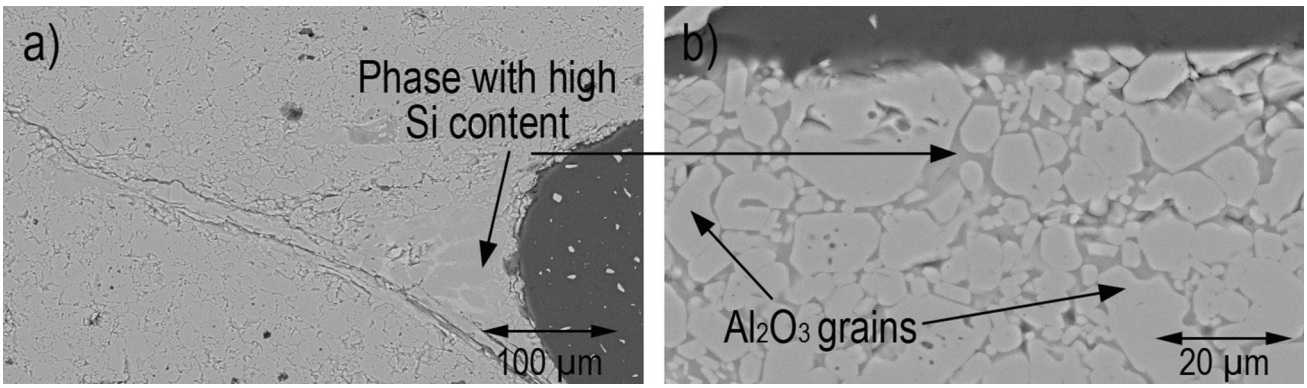

Fig. 8—SEM images (backscattering mode) of alumina foams coated with spodumene 1 (thermally treated at 1400 °C) (*a*) magnification 200×, (*b*) magnification 1000×.

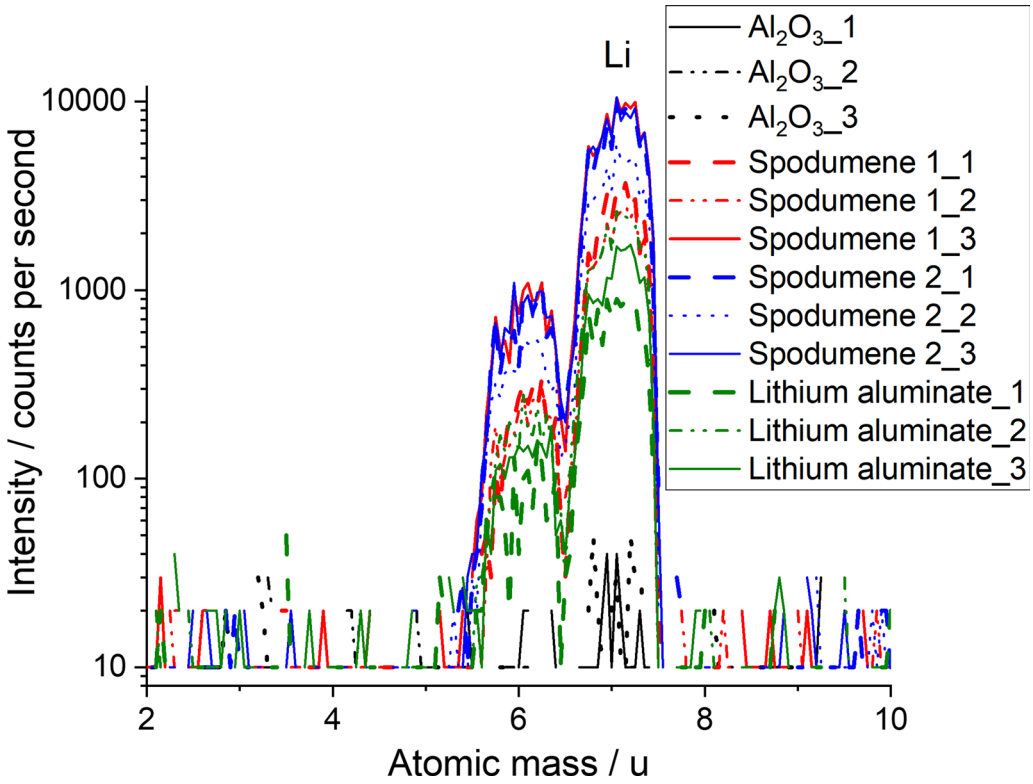

Fig. 9—Mass spectra (intensity as a function of atomic mass) of the coated and sintered substrates measured by SNMS.

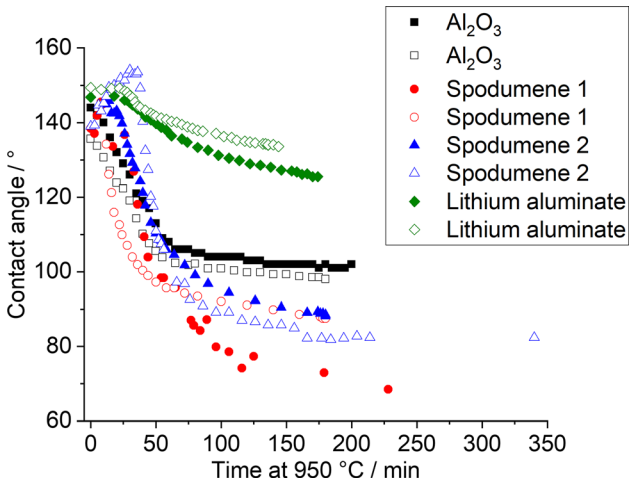

Fig. 10—Contact angle in dependence on time and substrate chemistry conducted with conventional sessile drop measurement at 950 °C and vacuum (Measurement Spodumene 1 was presented by Fankhänel[7]).

contact angle. At the beginning of the holding time, the contact angle is > 140°, *i.e.*, relatively high caused by the oxide layer affecting the contact angle. Due to the temperature of 950 °C and the vacuum, the contact angle started to decrease rapidly after reaching the maximum temperature. After around 45 minutes at 950 °C, the decrease rate was slower and reached an almost stable value of approximately 100° after 125 minutes. This behavior was also described by Bao *et al.*[26] for the system of alumina and pure aluminum. On the contrary, the lithium-containing substrates did not reach a quasi-stable value indicating a reactive system. Also typical for reactive systems is the low repeatability of the measurements of the same sample type. The measurements showed lower contact angles for the spodumene substrates (spodumene 1 and spodumene 2) than for alumina. The lithium aluminate-containing substrates possess a higher contact angle, see Figure 10 and Table III. The samples after the measurement showed no visible changes of the alumina and the lithium aluminate substrates, whereas the two spodumene types show clear gray and yellow discoloration of the surface, see Figure 11. The reaction of the two spodumene types, in contrast to the missing reaction for the lithium aluminate, hints at the strong influence of the silicon. The contact angle measurements between spodumene 1 and AlSi5Mg were presented by Fankhänel *et al.*[7] for the first time and were included in this work for the sake of completeness. Fankhänel *et al.*[7] complemented the sessile drop tests with SEM analysis of the interface between spodumene and AlSi5Mg, yielding a reaction layer.

The drawback of the conventional sessile drop tests for aluminum melt is the high temperature of ≥ 950 °C, which, as noted, must be used for the decomposition of the oxide skin. Typical operating temperatures of aluminum melt filtration are between 690 and 730 °C and lower than the temperature of the conducted sessile drop tests. Therefore, a modified sessile drop method using an adapted capillary purification technique was used enabling an oxide skin free drop at temperatures used for the processing of aluminum. The glossy surface

Table III. Contact Angles of the Sessile Drop Measurements

	Contact Angle/°				
	Conventional Sessile Drop Test (950 °C and Vacuum, After 150 Min		Sessile Drop Test With Capillary Purification Setup (< 730 °C , Directly After Dropping)		
	Measurement 1	Measurement 2	Left side	Right side	Temperature at Dropping/ °C
Al_2O_3	102	99	128	135	609
Al_2O_3 + spodumene 1	75	85	94	93	730
Al_2O_3 + spodumene 2	90	90	99	107	681
Al_2O_3 + lithium aluminate	133	127	144	147	603

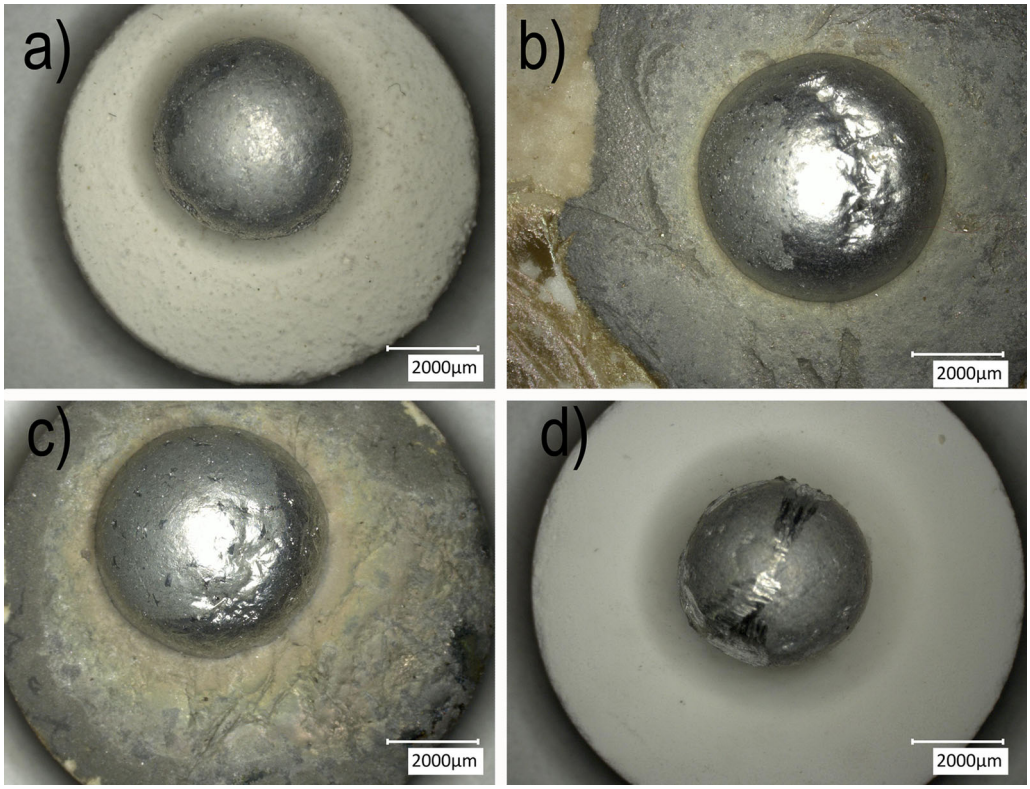

Fig. 11—Light microscopic images of samples after conventional sessile drop tests at 950 °C with different substrate materials (*a*) alumina, (*b*) coated with spodumene 1, (*c*) coated with spodumene 2, and (*d*) coated with lithium aluminate.

of the droplet is a hint of an oxide-free skin, see Figure 12. The contact angles were measured immediately after dropping. Nevertheless, the dropping took place at different temperatures (alumina substrate at 609 °C, spodumene 1 at 730 °C, spodumene 2 at 681 °C, and lithium aluminate at 603 °C) having a significant influence on the contact angle, see Table III. Due to the absence of a mechanical trigger, the dropping temperature cannot be chosen by the operator. It is notable that a comparison between the different materials is difficult due to the different temperatures at the fall of the drop. The main task of this sessile drop test with capillary purification setup was to identify whether reactions observed after 180 min at 950 °C (see Figure 11) will take place at lower temperatures as well. The appearance of the substrate/aluminum couple shows apparent differences after the test with capillary purification compared with the conventional sessile drop test—no surface changes of the spodumene substrates (spodumene 1 and spodumene 2) are visible for the test with capillary purification, see Figure 13. The samples of all four tests exhibit a white surface comparable to the appearance before the test, indicating that no visible reactions were observable at temperatures relevant for aluminum processing. The interface between aluminum and substrate was not examined.

D. *Casting Trials and Evaluation of the Porosity in the Cast Aluminum Samples*

Finally, the influence of lithium-containing filter surfaces on the hydrogen porosity was targeted.

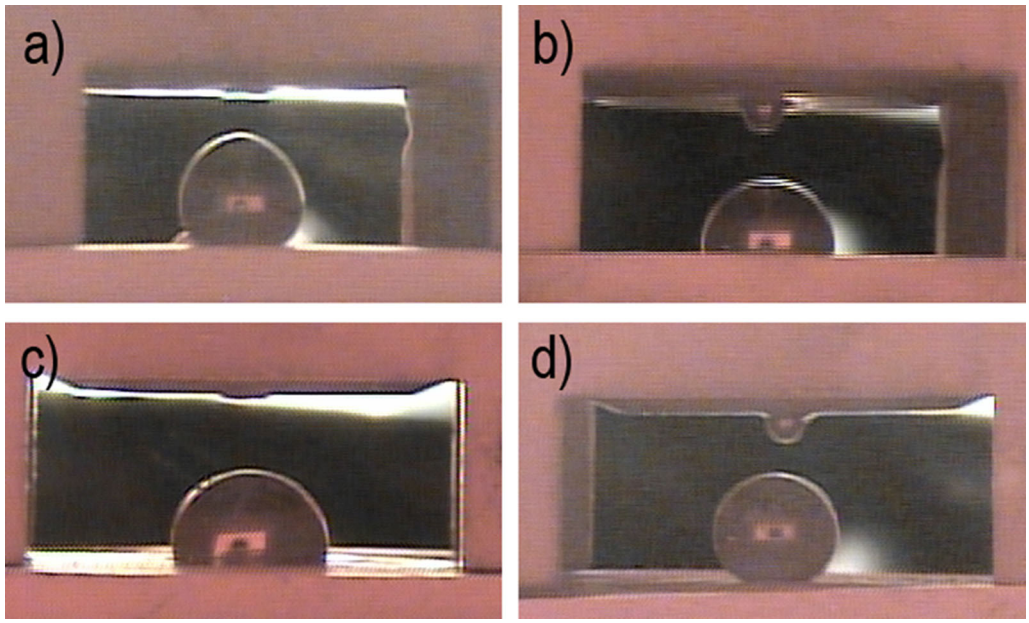

Fig. 12—Wetting tests with capillary purification technique with different substrate materials (*a*) alumina dropping at 609 °C, (*b*) spodumene 1 dropping at 730 °C, (*c*) spodumene 2 dropping at 681 °C, and (*d*) lithium aluminate dropping at 603 °C.

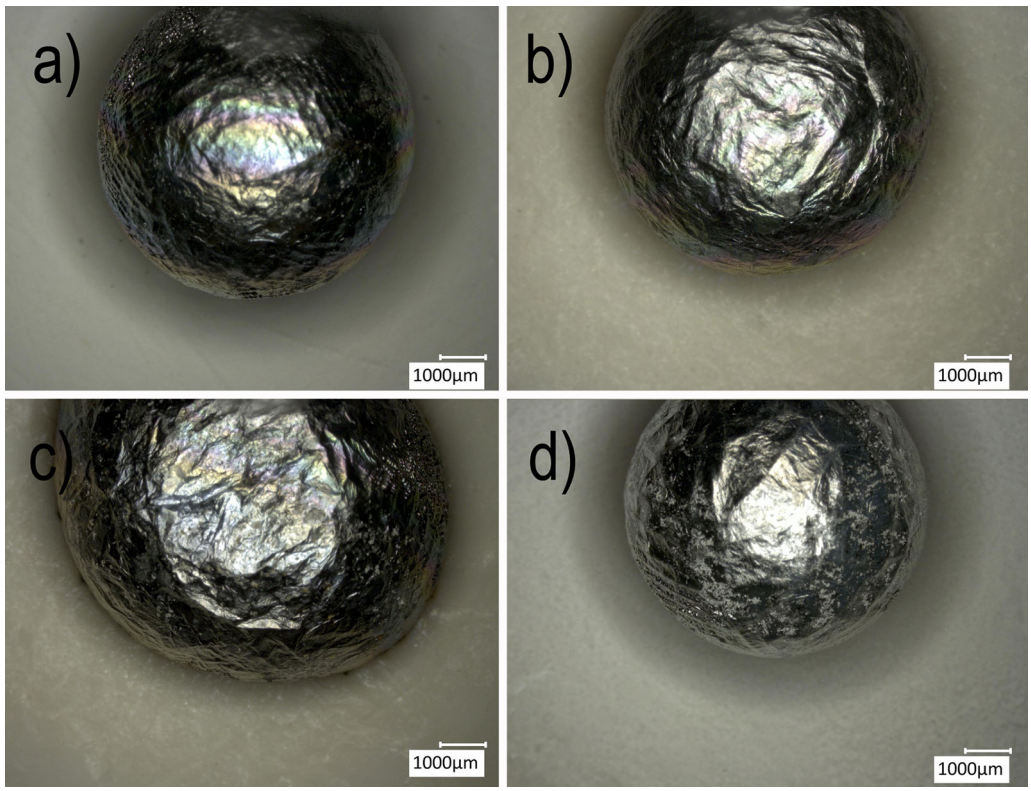

Fig. 13—Samples after wetting tests with capillary purification technique (*a*) alumina, (*b*) spodumene 1, (*c*) spodumene 2, and (*d*) lithium aluminate.

The cast aluminum samples were examined regarding their porosity, whereby every sample type was cast three times. There are different reasons for the formation of porosity in cast aluminum. Due to the lower hydrogen solubility in solid compared to liquid aluminum, present hydrogen is rejected from the solution and forms pores, either large primary (interdendritic) pores or small secondary pores (1–2 μm).[1] Further reasons for the formation of pores are other solved gases as well as shrinkage caused by the density difference between liquid and solid aluminum. In this study, the detected pores were not examined regarding their origin. Due to

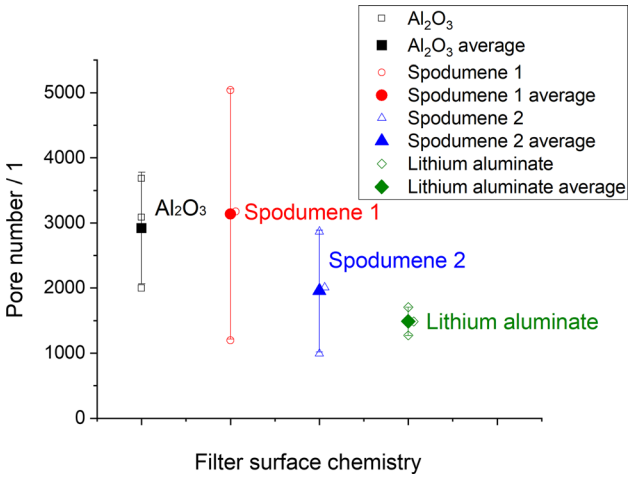

Fig. 14—Pore number in dependence on the filter surface chemistry (analyzed area 8.4 × 23.4 mm^2).

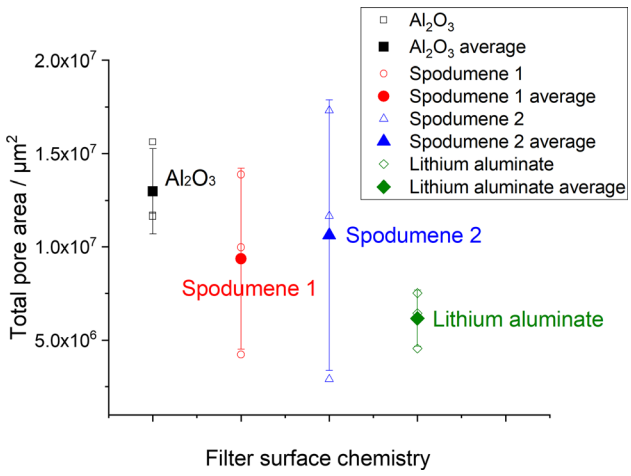

Fig. 15—Total pore area in dependence on the filter surface chemistry (analyzed area 8.4 × 23.4 mm^2).

the comparable trial conditions and the same aluminum alloy, it can be assumed that the amount of shrinkage pores is comparable for all trials and therefore observed differences in the measured porosity can be traced to differences in the hydrogen content of the aluminum. Figures 14 and 15 show the large scatter of pore number and pore area in dependence on the used lithium-containing raw material. The differences between the different sample types are within the standard deviation and so the differences are not significant. Nevertheless, the low scatter and the low average values of the lithium aluminate sample are noticeable.

In the next step, the distribution of the area-equivalent pore radii of the different sample types were measured by light microscopy. These distributions of the pore radii possess a large scatter within one sample type, see Figure 16. It was observed that the differences between the different sample types are not significant compared to the differences between the repeated measurements.

The quantitative analysis of the computed tomography data only allows the quantification of pores larger than 100 μm, but within a larger volume of approximately 14 × 27 × 42 mm^3 compared to the analysis of a 2D cross-section by means of light microscopy. The evaluation of the computed tomography measurements shows that there are significant differences within one sample type in dependence on the casting trial, comparable to the results of the light microscopic inspection, see Figure 17. It is noticeable that the position of pores > 100 μm was rather random. Due to a lack of repeatability, no quantitative evaluation of the pores detected by computer tomography was conducted. Under the specified conditions of the performed cast trials, no definite conclusion can be reached with regard to the influence of the lithium-containing filter surfaces on the pore size distribution that could be detected. It should be pointed out that the observations of this study are the result of the specific trial parameters, for example, filter roughness, used aluminum alloy and hydrogen content of the melt. Trials conducted under different conditions might reveal different results. Further investigations are necessary.

IV. CONCLUSIONS

To reduce the formation of hydrogen pores in cast aluminum, lithium-containing ceramic foam filters were tested. The lithium approach takes advantage of the affinity of lithium to hydrogen, whereby spodumene (a lithium aluminum silicate) and lithium aluminate were used as lithium providers.

Within the scope of this study, the tested lithium-containing raw materials were analyzed regarding lithium content, melting temperature, and behavior on an alumina substrate. In the next step, alumina skeleton foams were coated with the lithium-containing material (spodumene), dried, sintered, and investigated with regard to the bending strength.

The investigations revealed that all spodumene coatings had a significant negative influence on the bending strength of the foams when a certain level of spodumene is exceeded. This is explainable by the intrusion of the spodumene into the alumina matrix of the skeleton foam which was proven with the help of SEM analysis. Two sessile drop tests at different temperatures (730 and 950 °C) were conducted, verifying the significant influence of the temperature on the reaction between the spodumene and the AlSi7Mg. At 950 °C, reactions between the lithium-containing materials and the aluminum are visible with the eye whereas no reactions at 730 °C were observed.

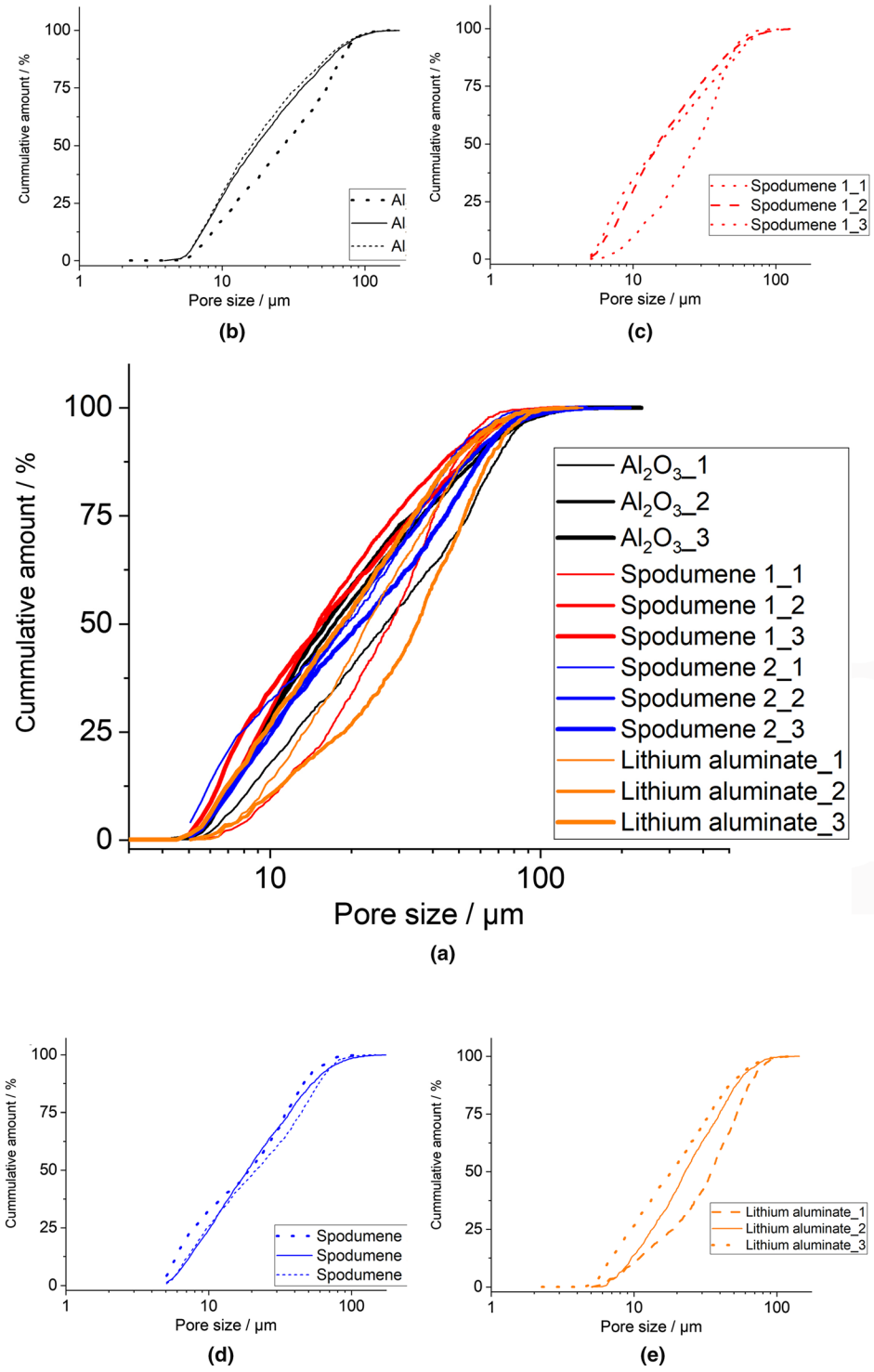

Fig. 16—Pore size distribution of the aluminum samples after the casting trials depending on the filter material (*a*) overview, (*b*) alumina, (*c*) spodumene 1, (*d*) spodumene 2, and (*e*) lithium aluminate.

In the last step, the effect of the lithium-containing open foam filters were tested with casting trials with alumina ceramic foam filters coated with raw materials with different amounts of lithium. The amount and size of hydrogen pores in the cast aluminum were evaluated by light microscopy and computer tomography. The analyzed pore size distributions in the aluminum show a large scatter which does not allow determining a proximate influence of the lithium-coating at the ceramic foam filter on the hydrogen porosity in the cast aluminum—*i.e.*, an influence of the lithium on the hydrogen pores was not detectable.

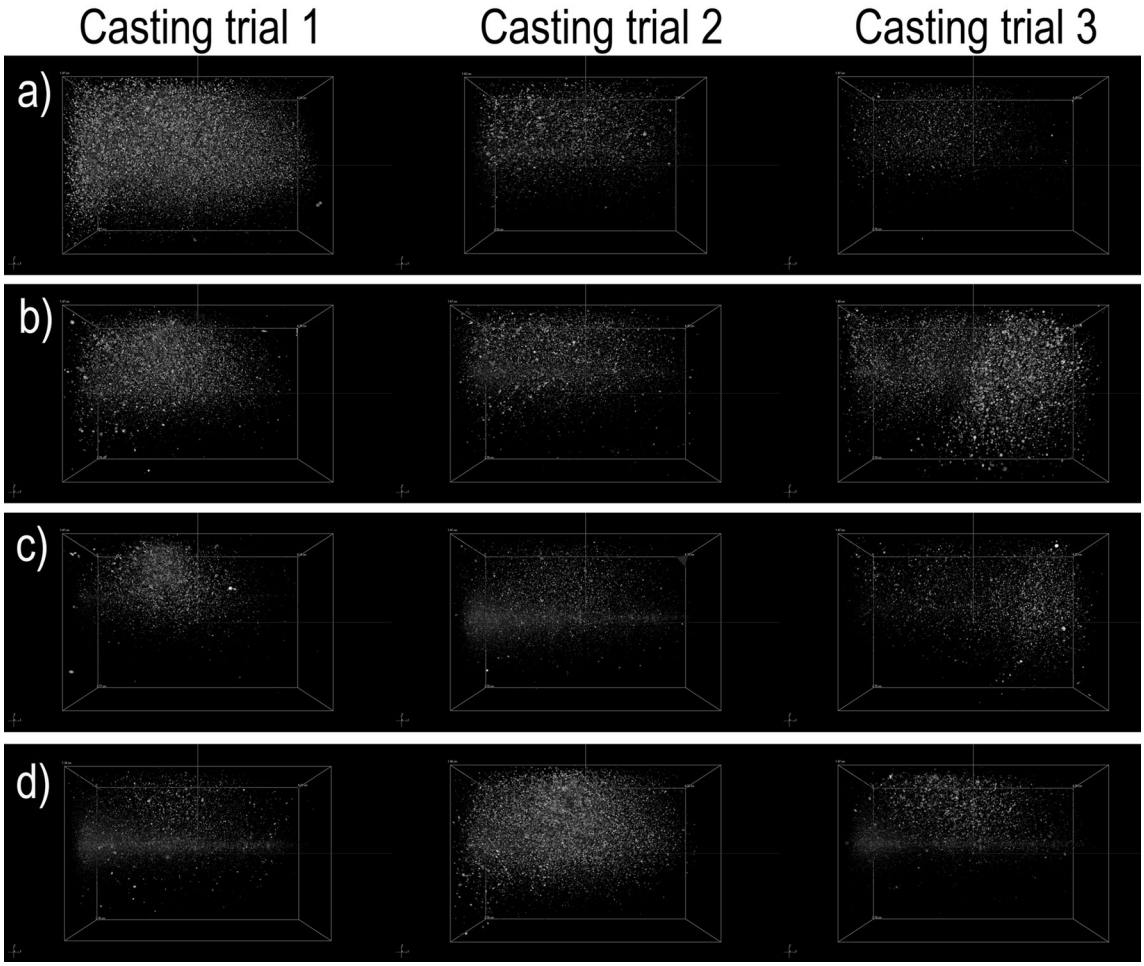

Fig. 17—Pores > 100 μm of the casted samples measured by CT depending on the filter material (*a*) alumina, (*b*) spodumene 1, (*c*) spodumene 2, and (*d*) lithium aluminate.

ACKNOWLEDGMENTS

The authors would like to thank the German Research Foundation (DFG) for supporting these investigations as part of the Collaborative Research Centre 920 "Multi-Functional Filters for Metal Melt Filtration—A Contribution towards Zero Defect Materials" (Project-ID 169148856) sub-projects A02, C06, and S01. The authors would also like to acknowledge the support of Mr. Gert Schmidt.

CONFLICT OF INTEREST

The authors declare that they have no conflict of interest.

FUNDING

Open Access funding enabled and organized by Projekt DEAL.

REFERENCES

1. E.J.T. David: *The Effects of Hydrogen in Aluminium and Its Alloys*, Maney Publishing, Leeds, 2004.

2. M. Tiryakioğlu: *Metals*., 2020, vol. 10, p. 368. https://doi.org/10.3390/met10030368.
3. A.J. Gerrard: Inclusions and Hydrogen and Their Effects on the Quality of Direct Chill Cast and Flat Rolled Aluminium Alloys for Aerospace Applications, Thesis 2014, University of Birmingham.
4. D.E.J. Talbot: *Int. Metall. Rev*., 1975, vol. 20, pp. 166–84.
5. B. Fankhänel, S. Grötz, and M. Stelter: *World Metall. Erzmetall*., 2019, vol. 72(1), pp. 1–7.
6. B. Fankhänel, J. Hubálková, C.G. Aneziris, M. Stelter, and A. Charitos: *Adv. Eng. Mater*., 2021, https://doi.org/10.1002/adem.202100579.
7. B. Fankhänel, M. Stelter, C. Voigt, and C.G. Aneziris: *Metall. Mater. Trans. B*., 2015, vol. 46, pp. 1535–41. https://doi.org/10.1007/s11663-015-0307-0.
8. M. Okrusch and S. Matthes: *Mineralogie-Eine Einführung in die spezielle Mineralogie, Petrologie und Lagerstättenkunde*, Springer, Berlin, 2014. https://doi.org/10.1007/978-3-642-34660-6.
9. L.N.W. Damoah and L. Zhang: *Metall. Mater. Trans. B*., 2010, vol. 41B, pp. 886–907.
10. M. Badowski and W. Droste: *Light Metals*., 2009, vol. 4, pp. 701–06.
11. A. Pelss: *Light Metals*., 2020, vol. 54, pp. 944–50.
12. H. Oechsner: *Thin Film Depth Profile Anal*., 1984, vol. 15, pp. 63–85.
13. H. Oechsner, W. Bock, M. Kopnarski, and M. Müller: *Microchim. Acta*., 2000, vol. 133, pp. 69–73.
14. H. Oechsner: *Thin Solid Films*., 1999, vol. 341, pp. 105–08.
15. A. Bianconi, R. Bachrach, S. Hagstrom, and S. Flodström: *Phys. Rev. B*., 1979, vol. 19, pp. 2837–43. https://doi.org/10.1103/PhysRevB.19.2837.
16. N. Eustathopoulus, M.G. Nicolas, B. Drevet: Wettability at High Temperatures, Pergamon, 1999; ISBN: 9780080421469.
17. C. Voigt, L. Ditscherlein, E. Werzner, T. Zienert, R. Nowak, U. Peuker, N. Sobczak, and C.G. Aneziris: *Mater. Design*., 2018, vol. 150, pp. 75–78.
18. C. Voigt, J. Hubálková, T. Zienert, B. Fankhänel, M. Stelter, A. Charitos, and C.G. Aneziris: *Materials*., 2020, vol. 13, p. 20203962.
19. N. Sobczak, M. Singh, and R. Asthana: *Curr. Opin. Solid State Mater. Sci*., 2005, vol. 9, pp. 241–53.
20. P. Shen, H. Fujii, T. Matsumoto, and K. Nogi: *J. Am. Ceram. Soc*., 2004, vol. 87(7), pp. 1265–73.
21. P. Malczyk, T. Zienert, F. Kerber, C. Weigelt, S.O.H. Sauke, and C.G. WAneziris: *Materials*., 2020, vol. 13, p. 4737. https://doi.org/10.3390/ma13214737.
22. A.F. Stalder, G. Kulik, D. Sage, L. Barbieri, and P. Hoffmann: *Colloids Surf. A*., 2006, vol. 286, pp. 1–3.
23. H. Salmang, H.t Scholze: Keramik 2006 ISBN 978-3540632733, pp. 264–66.
24. J.F. Shackelford and R.H. Doremus: *Ceramic and Glass Materials Structure, Properties and Processing*, Springer Science & Business Media, New York, 2008.
25. M. Chen, F. He, and J. Shi: *J. Eur. Ceram. Soc*., 2019, vol. 39(15), pp. 4988–95. https://doi.org/10.1016/j.jeurceramsoc.2019.07.032.
26. H. Jenett: Analytiker Taschenbuch 16 1997 ISBN 978-3540620099, pp. 43–117.
27. U.C. Schmidt, M. Fichtner, J. Goschnick, M. Lipp, and H.J. Ache: *Fresenius' J. Anal. Chem*., 1991, vol. 341, pp. 260–64. https://doi.org/10.1007/BF00321560.
28. S. Bao, K. Tang, A. Kvithyld, M. Tangstad, and T.A. Engh: *Metall. Mater. Trans. B*., 2011, vol. 42B, pp. 1358–66.